

Effect of non-circular nozzle shape on impingement cooling characteristics

Yavuzer Karakuş*, Araz Jabbarlı and Duygu Erdem
Istanbul Technical University
Faculty of Aeronautics and Astronautics

Abstract

Turbine inlet temperature is a parameter which affects the efficiency of a gas turbine engine. The higher this value is, the efficient the engine. Today turbine blades face temperatures in the order of 1500K which is far above the endurance limit of the blade material. Cooling is the primary method to reach these temperatures. "Impingement cooling" is an effective cooling technology used in gas turbines. In this study the flow and heat transfer characteristics of single impinging jets which issue from different nozzle geometries, i.e. lobed, were studied. The effect of nozzle exit geometry change is the main interest of the study. CFD analysis were conducted using v^2f RANS turbulence model. Results were evaluated from a perspective of relations between flow and heat transfer.

1. Introduction

Jet impingement is the fluid stream that is extracted from the different nozzle geometries with high velocity to the target surface which can be flat or curved. The notable characteristics of the jet impingement is the inherit properties of simple jet flow, the high rate of momentum and mass transfer or ample mixing characteristic. This feature of flow makes the jet impingement popular in application to the numerous heat transfer devices. In addition, the main attractive part for the designers is the controllability of the area and the distribution of thermal exchange. There are a lot of examples of heat transfer devices in industry that uses the jet impingement cooling. To illustrate, the annealing of metal, the tempering of glass sheets, the cooling of turbine blades, the chemical vapor deposition, propulsion jet-to-flaps interaction in STOL aircraft and thermal anti-icing systems of wings. [1]

The key parameters that affect the heat transfer performance of a single impinging air jet are Reynolds number, Prandtl number, jet diameter, jet-to-target spacing, confinement and nozzle geometry. There are countless experimental and numerical works which investigated the effect of these parameters on impingement jets.

O'Donovan and Murray [2] investigated the heat transfer distributions from a heated flat surface which is subjected to the unconfined impinging air jet from a pipe for Reynolds number from 10000 to 30000 and non-dimensional surface to jet exit spacing, H/d , from 0.5 to 8. They experimentally determined the time averaged surface heat transfer data including mean and root-mean-square Nusselt number distributions for the various jet impingement configurations. The results showed that the maximum heat transfer occurred at the lowest jet-to-target spacing H/D of 0.5, due to the low heat transfer fluctuation in stagnation zone. Both time averaged and fluctuating Nusselt numbers peak in the radial distance r/D of 1.6 for H/D of 0.5 but it decreases as the spacing increases. In the second part of the paper, the results are presented in two sections which are free jet fluid velocity and wall jet flow. The measurements that were carried out by Micro-Foil, Hot Film and Laser Doppler Anemometry, revealed that there are three dominant peaks ranging from 0.6 to 1.6, are given in terms of Strouhal number. The highest number is the roll up of the vortices, on the other hand, the lowest one is the merging process of vortices. [3]

Moreover, the investigation also considered the wall jet region where the vortices resulted from the merging process begins to be broken down as the wall jet flow undergoes transition to fully turbulent flow. Overall, the high heat transfer was observed in the region where the velocity fluctuations normal to the impingement surface and also as the height of the nozzle changes from 0.5 to 2 diameters, the mean velocity in the axial and radial direction does not change significantly, the only difference between these heights is the stage of the vortex development. [3]

Carlomagno and Ianiro [4] presented a review where they pinpointed and wrote different experimental and numerical contributions over the last 50 years on the complex flow structures of jet impingement. They gave a special attention to the some particular techniques in the field of modern experimental thermo-fluid-dynamics which are infrared thermography, particle image velocimetry (PIV) and along with the recently developed tomographic PIV. Analogies between experimental and recently developed computational methods have been made in the paper. The review explained the basic impinging jet flow physics with the details where it mentioned the regions of the emerging jet from the round exit and considered that the jet to plate spacing is large.

In addition to the physical characteristics of the jet flow, Carlomagno and Ianiro [4] also gave a special attention to the specific experimental techniques in thermo-fluid-science. They mentioned the relevant modern techniques in the field which are infrared thermography, particle image velocimetry (PIV) and recently developed tomographic PIV. Outcomes that are obtained from the visualization were compared with the recent advanced computational methods such as RANS, instantaneous 3D flow field with LES and DNS.

The recent comprehensive study about conjugate heat transfer process of impingement jet was done by Xiao et al. [5]. The study was carried out computationally to basing on a validated CFD model of free-air-jet that discharges from a round nozzle and impinges perpendicularly onto a solid plate with uniform heat flux boundary condition on heated surface. The previous numerical studies related to impingement jet did not consider the conjugate heat transfer which brings the additional complexity to the problem. The model which was proposed on this paper was a free-air-jet that discharges from a round nozzle and perpendicularly impinges onto the center of a disk. The model was solved with ANSYS ICEM-CFD. As a turbulence model The Shear-Stress Transport (SST) $k-\omega$ model was used. The analyses were done assuming non-conjugate and with conjugate heat transfer cases. The first part of the analysis showed that the computational method perfectly predicts the heat transfer distribution by comparing with the available experimental results. [2] The same simulations were performed for conjugate heat transfer case. Due to the different levels of thermal coupling, the global Nu for the conjugate cases were downgraded.

Han and Goldstein [6] briefly reviewed the single and multiple circular impinging jets and also mentioned the other affecting parameters like concave surfaces, cross flow, impingement angle and finally the rotational effect. The review concluded that the further investigation can be done to analyze the combined effect of the above mentioned parameters.

As an effective parameter of the impingement heat transfer, cross flow was analyzed by Bouchez and Goldstein [7]. The investigation was done with an impinging jet on a wall of wind-tunnel where the jet ejected from the circular tube, is subjected to a cross flow of air with several different blowing rate or mass flux ratio and also the investigation was done with two different jet-to-target spacing. These experiments were visualized and presented with images. . According to the paper, the high blow rate makes a strong interaction at the impingement surface which leads to the creation of a recirculation zone upstream of the stagnation point. However, in the opposite case, with the moderate blowing rate the same recirculation and mixing zone with the stagnation point moves downstream. Another survey was done by the Jambunathan et al. [8] about heat transfer data for single circular jet. The authors gave a detailed survey about the influential parameters of heat transfer coefficient in the impinging air jet. They concluded that the common active parameters are Reynolds number, jet-to-target spacing (H/d), non-dimensional radial distance (x/d) and the Prandtl number.

Glynn et al. [9] performed experimental investigation on single circular jet with varying jet diameter, Reynolds number and jet to target spacing. The investigation also conducted with the different fluid as water. The local and full-field heat transfer coefficient was analyzed. According to the results, for a single axisymmetric submerged and confined air and water jets, the area averaged heat transfer increases with decreasing the jet diameter because as the diameter decreases, the jet velocity increases. Additionally, Reynolds numbers and jet-to-target spacing were changed and investigated respectively, the results showed that as the jet-to-target spacing increases the heat transfer coefficient decreases. The same trend was observed in all combinations.

In order to investigate the confinement effect on single circular air jet San et al. [10] conducted an experiment where they experimented the jet flow in four different jet diameter for the Reynolds number ranging from 30,000-67,000 and constant spacing. The results showed that the jet diameter is a strong factor affecting the Nusselt number because for the same Reynolds number, the smaller jet-hole diameter resulted in a small Nusselt number. Another greatly affecting factor in this case was flow recirculation and mixing on the impingement surface.

Going one step further in the jet impingement cooling Yan and Saniei [11] investigated the heat transfer in an obliquely impinging air jet to a flat plate. They conducted an experiment with an air jet impinging obliquely from a circular nozzle using the preheated wall transient liquid crystal technique. The angles that jet strikes the target plate was taken as 90° , 75° , 60° and 45° . For the sake of comparison two different Reynolds number of 10,000 and 23,000 were considered. Another varied key parameter in the measurement was jet-to-target spacing. Four values were considered 2, 4, 7 and 10. The results showed that the local heat transfer showed a non-axisymmetric form and also as the jet-to-target spacing become smaller asymmetry becomes more evident.

Besides all the previously talked parameters, array of jet is another key parameter that affect the heat transfer which was considered by Jennerjohn et al [12]. The conducted experiment considered the combined effects of hole array spacing, jet-to-target spacing and Reynolds number on the local heat transfer. The results showed that in overall, the local Nusselt numbers generally increase at each location of the target surface as either the Reynolds number increases, or as the spanwise and streamwise hole spacing decreases.

Colucci and Viskanta [13] investigated the effect of hyperbolic nozzle geometry on the local heat transfer coefficients for confined impinging air jets. They considered low nozzle-to-plate spacings from 0.25 to 6 and the Reynolds numbers in the range of 10,000 to 50,000 for two different confined, hyperbolic nozzle. As expected, with the increase of the Reynolds number for two of the geometry, the Nusselt number increases. Another nozzle configurations were proposed by the Gulati et al. [14]. They investigated the combined effect of nozzle geometry, jet-to-plate spacing and Reynolds number on the local heat transfer distribution on submerged air jet. The three different nozzle geometries were used which are circular, square and rectangular. For visualizing the local heat transfer, infrared thermal imaging technique was used. The results showed that for all the nozzle geometries the effect of Reynolds number is same. As the Reynolds number increases the heat transfer rate increase. In this context, the square and circular jets showed similarity. Overall, up to the jet-to-target spacing of 6, Nusselt number distribution is higher for rectangular geometry than circular and square. In addition to the square and rectangular geometry Kanamori et al. [16]. Investigated the non-circular polygons which are polygons with 3 to 6 sides. The results were visualized using the hydrogen bubbles. They concluded that sharp edge orifice has more effect on heat transfer compared to other configurations. The sharp edge orifices greatly influence velocity profile at nozzle exit and induces higher rate of turbulence intensities in the jet. This greater rate of turbulence intensity results is more efficient heat transfer. There is also a cross-shaped nozzle which was used by Sodjovi et al. [17] They used plane cross-shaped and hemispherical nozzle. Particle image velocimetry (PIV) were used to visualize the results of impinging jet. The radial distribution of mean streamwise velocity and spanwise turbulent intensity was measured using PIV method. The results showed that introducing a curvature to the surface, completely changed behavior of the jet flow generated. Since the application was done for the HVAC application, the observed results presented as mass transfer. Overall, the hemispherical cross-shaped nozzle showed a better local and global mass transfer compared to the plane cross-shaped and circular nozzle. Another nozzle geometry was proposed by Martin and Buchlin [15]. They conducted experiment with the lobed geometries. They used three and four lobed nozzles. The quantitative infrared thermography associated with the thermofoil technique was used. They concluded that for the low jet-to-plate spacings at $z/d \leq 1$, the three lobed nozzle showed a better performance than other nozzle geometries that was proposed previously by Gulati et al. [14]. However, as spacing increases and exceeds 7, the four lobed nozzle yields better performance. The present paper also deals with heat transfer analysis of the lobed nozzle. This time 4, 6 and 12 lobed nozzles are analyzed. The analyses are conducted both numerically and experimentally.

2. Method

2.1. Geometry

Lobed straight nozzles are the focus of this study. 4, 6 and 12 lobed nozzles were selected as the exit geometry of the nozzle. Circular nozzle was used as the reference case with the literature. Sketches of the exit geometries are shown in Figure 1. Flow parameters were determined following the specification of the geometry. Equivalent jet diameter (D), which is the diameter of the circular nozzle with the same area, calculated for all nozzles were taken to be the same. D is the characteristic length used throughout this study as hydraulic diameter will change for each nozzle. Jet to impingement plate spacing (Z/D) is specified as 5 in the light of past work. Reynolds Number (Re) based on D was specified as 50000. The flow was assumed to be incompressible for this Re . Heat flux is determined to be 1000W/m^2 for the heat transfer investigations.

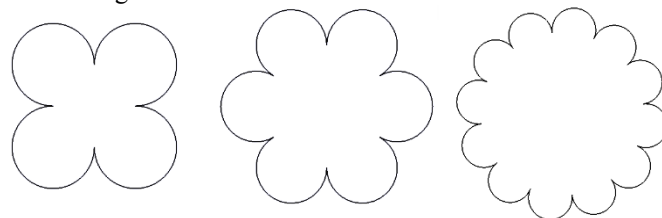


Figure 1: Sketches of the nozzle exit geometries

After the specification of the exit geometries, geometry of the flow domain was specified. This domain consists of a settling chamber, a nozzle plate at the exit of the settling chamber and the impingement table where the jet impinges and heat transfer occurs. With these parameters in mind an experimental set up was designed and CAD drawings were prepared. Also the model of the flow domain which also includes a part of the surrounding ambient air was drawn. A section of the flow domain for the 4 lobed nozzle is shown in Figure 2.

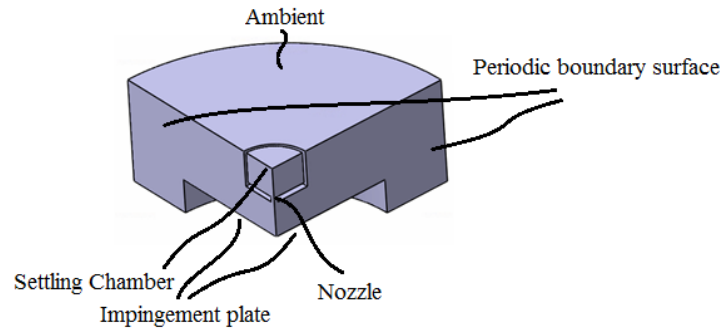


Figure 2. A section of the flow domain of the 4 lobed nozzle case

2.2. Experimental Set up

Experimental set up consists of a pressure source which is the low-pressure compressor of the Trisonic Research Laboratory. Pressurized air is sent to settling chamber which has a port for pressure measurement. Settling chamber ends with an orifice plate where the straight nozzle is. Jet issuing from the nozzle impinges on the impingement plate. The distance of the orifice plate can be changed for different plate to nozzle distance values. Impingement plate is made of three sections one of which is interchangeable. The outer ring is fixed to the legs and it has the angle protractor on it. Inside this ring a circular plate which carries the pressure measurement plate or the heat transfer measurement plate. In this study only pressure measurement plate was used due to funding restrictions. Pressure measurement plate has pressure taps on perpendicular lines. All the pressure tapping lines starts from the center, with a spacing of $0.2 D$ but the first hole is at $0, 0.1D, 0.3D$ and $0.4D$. The domain can be scanned with $0.1D$ spacing on the radial direction. In this study $0.2D$ measurement interval was decided to be used. The set up was manufactured using laser cut acrylic and 3D printing. Resolution of the laser cutter is 3% while 3D printer has a resolution of 4% of D . A pressure scanner was used to measure differential pressure with respect to the atmospheric pressure. Accuracy of the pressure scanner was 0.5% full scale.

2.3. Computational Fluid Dynamics Analysis

Flow domain for the CFD analysis was designed to be the same as the experimental set up. Domain consists of a circular settling chamber with an orifice plate and a circular impingement table. A wider volume is taken to model some part of the ambient. All the nozzles are axisymmetric so can be modeled as periodic sections. A slice of the flow domain which contains a lobe is taken as the domain to be used in the CFD. It also gives advantage in terms of computational expense.

CFD methods were evaluated to select the most convenient one to be used throughout the study. Reynolds-averaged Navier-Stokes (RANS), Large-Eddy simulation (LES) and direct numerical simulation (DNS) methods were evaluated. DNS is the most reliable one for resolving the flow field but it is the most expensive model to be used when compared with the other methods. LES is a more reliable method when compared with RANS as it solves the large eddies directly while modeling only the small eddies. But LES is still an expensive way to be used in the CFD calculations. RANS methods use turbulence models to resolve the turbulent flow thus need low computational resources. Using turbulence models puts limitations on the extent to which the flow field is resolved [18]. RANS turbulence models were evaluated as the computational resources available pointed out. Among the RANS turbulence models, v^2f model was selected. v^2f model is similar to $k-\epsilon$ but incorporates near-wall turbulence anisotropy and it is a low Re model that is valid up to the solid walls thus does not use wall functions [19]. v^2f model solves impinging jet flows very precisely, both flow and heat transfer values are close to experimental results [20]. Mesh was constructed using unstructured tetrahedral mesh with prism boundary mesh in near-wall sections. Boundary mesh sizes had been selected to provide the y^+ values needed for the turbulence model used. Periodic boundary condition of the CFD software was used. Mesh of the periodic face is shown in Figure 3. Here the prism boundary mesh can be seen in detail.

Following the preparation of mesh structure, mesh was transferred to the CFD code which has been determined to be used thorough the study. Convenient boundary types were assigned, such as a pressure inlet type on the settling chamber inlet, pressure outlet on the outer borders of the downstream part of the domain and wall type on the walls of the settling chamber and nozzle.

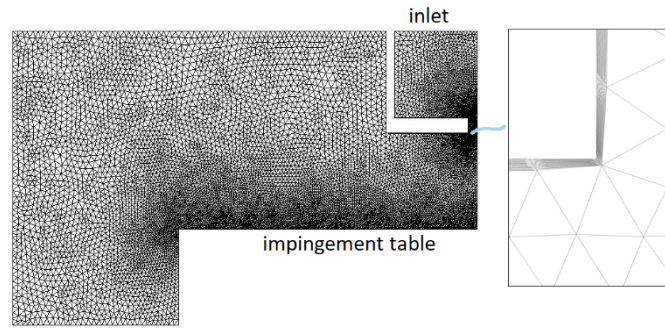


Figure 3: A view of the mesh used – periodic boundary

3. Results and Discussion

Boundary conditions are applied and results are obtained both experimentally and computationally. Parameters used for evaluating the flow and heat transfer are determined as the pressure coefficient, c_p , skin friction coefficient, c_f , and Nusselt number, Nu . Their formulations are given below. Here p is the static pressure on the wall, p_s is the ambient pressure and V_m is the mean velocity at the nozzle exit. τ_w is the wall shear stress. h is heat transfer coefficient and k is the thermal conductivity. of the fluid.

$$c_p = \frac{p - p_s}{\frac{1}{2} \rho V_m^2} \quad (1)$$

$$c_f = \frac{\tau_w}{\frac{1}{2} \rho V_m^2} \quad (2)$$

$$Nu = \frac{hD}{k} \quad (3)$$

Experimental and CFD results were compared on two regions. One of them is “intersection line” which passes through the intersection of two lobes and the center. The other one is “mid lobe line” which is the symmetry line of a lobe. Their positions are shown in Figure 4. θ changes as the number of lobes change. It is 45, 30 and 15 degrees for 4 lobed, 6 lobed and 12 lobed nozzles respectively. Circular nozzle is axisymmetric so data was taken from a line.

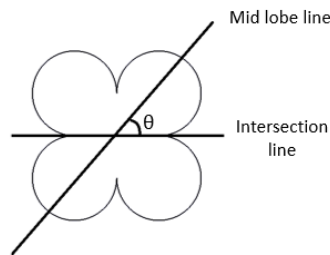


Figure 4: Positions of the intersection line and mid lobe line

Grid independence study was conducted to check if the solution is independent of the grid structure. Coarse mesh structure consists of 240627 nodes while fine mesh consists of 487807 nodes. Nusselt number distribution on intersection line was compared. Results are shown in Figure 5.

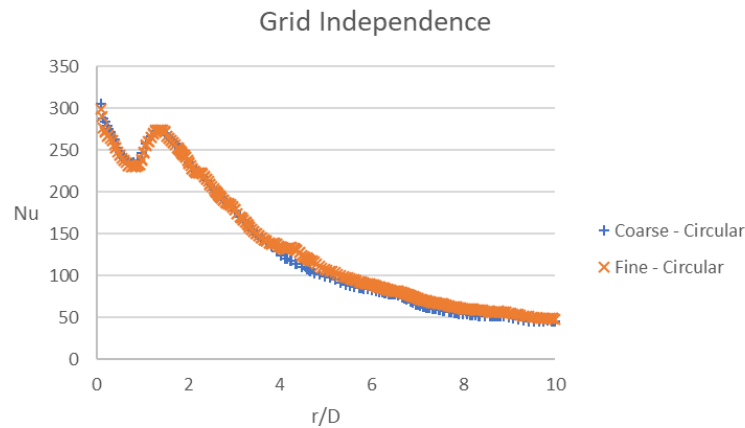


Figure 5: Grid independence study results

Pressure distribution, in terms of c_p is compared in Figure 6. $v2f$ model under-estimates the pressure distribution between $0.5D$ and $1.5D$ when compared to experimental results but then converges to the experimental results. Stagnation pressure and outer regions agree with the experimental results.

Nusselt number distribution for the circular nozzle case was compared with the data from literature. Correlation of [21] taken from [22] was used for r/D between 2.5 which is the lower limit and 10 . Heat transfer data of a circular impinging jet [23] of similar aspect ratio and same Z/D ratio was also used. But Re which were in our interest was 40000 and 60000 . These three data sets were used to evaluate the accuracy of the CFD approach. Figure 7 shows the data. CFD data shows a secondary peak which is a sign that it estimated a longer core region which is closer to the impingement table than experimental results show. $Z/D=5$ was known to be close to the interval where the potential core reaches its limits [24], this might be interpreted as a small drift.

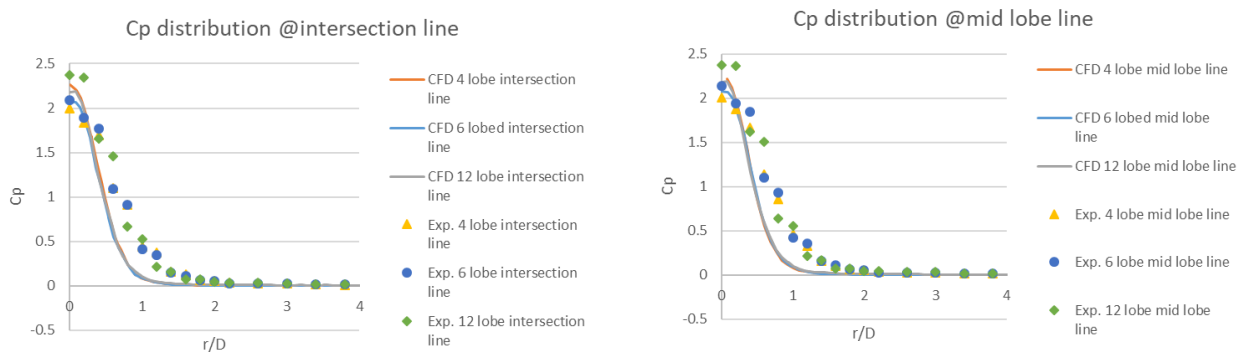


Figure 6: Pressure distribution on the intersection line (left) and mid lobe line (right), CFD and Experimental results

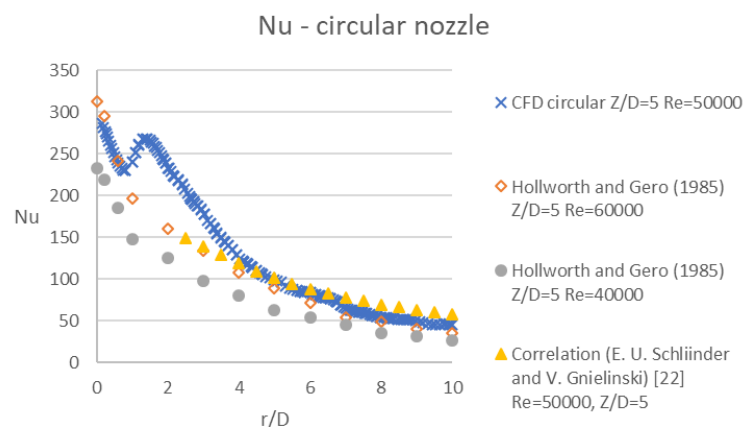


Figure 7: Comparison of CFD results (circular case) with data from literature

Switching to CFD results, Nu and c_f are the parameters considered. Nusselt number distribution of the three different cases are shown in Figure 8. Nozzle shape and circles having r/D ratios of 1, 3 and 5 are shown as cyan colored lines. Here it can be seen that the shape of the contours in the mid-section is similar to the exit geometry. Then profiles rotate half lobe angle and when moved outward they converge to a circular shape. But this translation is different for each geometry. Profiles for the 4 lobed geometry are more resistant to this change so change takes place slower. Profiles of 12 lobed nozzle makes this translation rapidly. At $r/D=5$ the effect of the exit geometry can still be seen for 4 lobed nozzle, while the same change has been realized at nearly $r/D=3$ for 12 lobed nozzle.

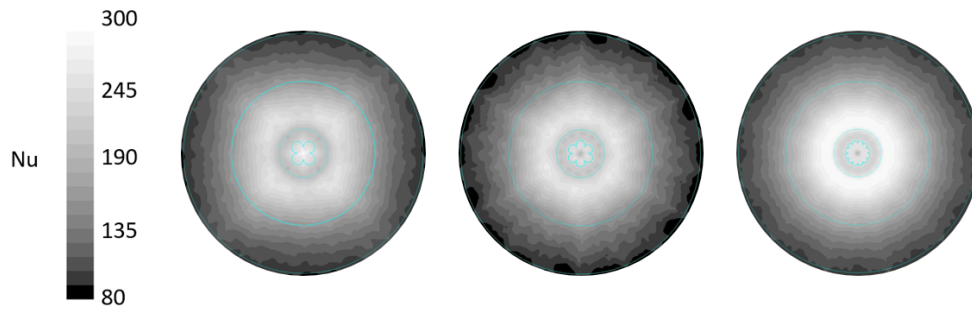


Figure 8: Nu distribution on the impingement plate for 4, 6 and 12 lobed nozzles (from right to left)

Nusselt number distribution was evaluated on intersection line and mid lobe line to see how the lobes effect the heat transfer performance. The results are shown in Figure 9. The distance between the intersection corner and the outer border of the lobes was highest for the 4 lobed case, that is why the difference was more. 6 lobed nozzle creates a closer distribution. 12 lobed case had nearly same distribution on intersection line and mid lobe line as these two lines are closer to each other than other geometries.

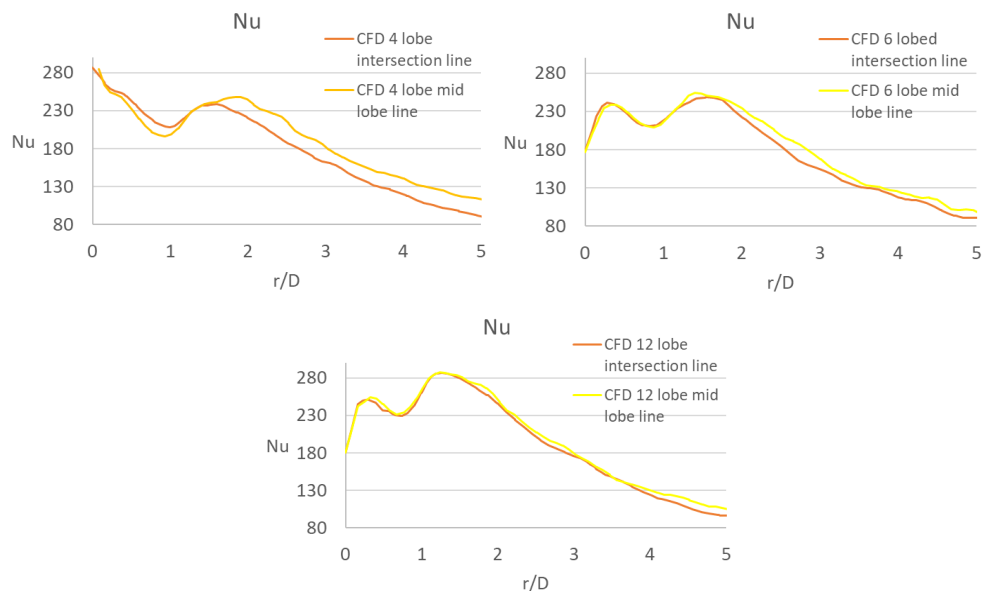


Figure 9: Nu distribution on the intersection line and mid lobe line

Skin friction coefficient shows the same tendency as Nu . Distribution of c_f is shown in Figure 10. It was considered that the effect of the nozzle geometry is conserved the most for 4 lobed nozzle but it is least conserved for the 12 lobed nozzle.

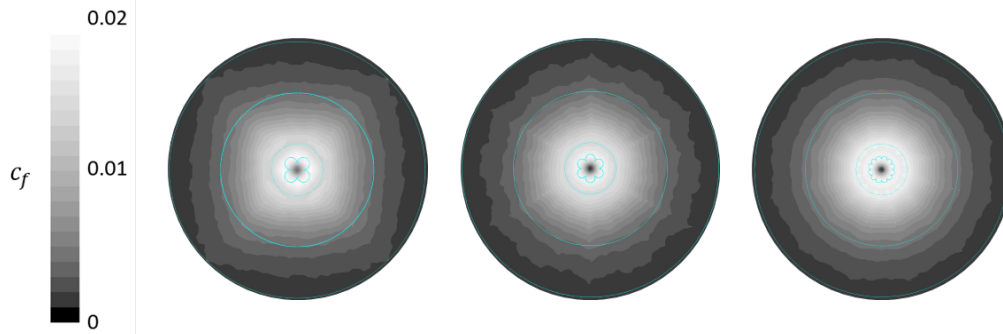


Figure 10: c_f distribution on the impingement plate for 4, 6 and 12 lobed nozzles (from right to left)

Average Nusselt number distribution on circular sections centered at the center of the impingement table is shown in Figure 11. Here all the circular sections start from the center of the impingement table and their radii are 0.5D, 1D, 1.5D, 2D, 2.5D, 3D, 4D and 5D respectively. If we consider the lobed geometries, 4 lobed geometry has the highest heat transfer near the center. But then has a decrease with two peaks until 2.5D where it meets the 6 lobed geometry. After that point 4 and 6 lobed geometries have a similar behavior and their Nu values are lower than 12 lobed. 6 lobed geometry has the lowest Nu value when compared with the other geometries. It meets 4 lobed at 1D and has a higher area averaged Nu value than 4 lobed between 1.5D and 2.5D. 12lobed starts in the middle but then has highest Nu values all over the range which is taken into consideration. Circular case is the reference in this study. Nu number is the highest at the center for circular jet but meets 12 lobed at 1D. Then follow the same trend with a slight lower heat transfer until 4D where 12 lobed and circular jets cause the same heat transfer performance. In an area with a radius of 5D 4 lobed, 12 lobed and circular jets results in the same heat transfer performance and 6 lobed jet has a slightly lower average Nu.

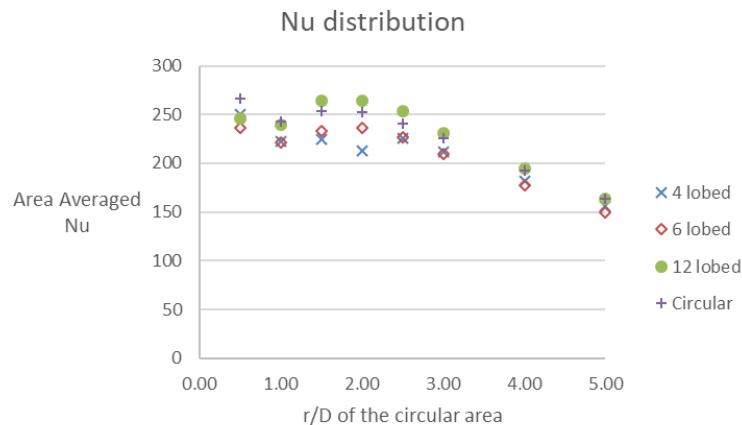


Figure 11: Average Nu values for different impingement areas

4. Conclusion

Impinging jets is a highly appreciated cooling method to be used in systems where both high heat loads and small volumes are present for the cooling system. Conventional production methods have only permitted for circular jets which are widely used in machinery. But due to the invention of new production technologies such as 3D printing of metals, non-circular nozzle exit geometries will be an option if they are more efficient. In this study, the effect of lobes on flow and heat transfer characteristics were studied for 4, 6 and 12 lobed nozzles.

Experimental and computational work was conducted and results were obtained. Pressure distribution on the impingement plate was taken from experimental results to evaluate the accuracy of the CFD results. Data of heat transfer performance was gathered from literature and used for the circular jet to check the accuracy of the CFD approach. Heat transfer distributions are taken from CFD analyses and compared for 4 lobed, 6 lobed and 12 lobed nozzles for Z/D ratio of 5 and Re of 50000. Results showed that 4 lobed, 12 lobed and circular nozzles have the same transfer performance which is slightly better than 6 lobed nozzle in an area of $r/D=5$. As the number of lobes increases, flow and heat transfer characteristics converges to a circular trend. But for $r<3D$ there is difference among different cases.

This study states that further investigation of lobed nozzle would be a contribution to cooling technology. Effect of Z/D, Re and nozzle aspect ratio might be the next step for this study. Also, it is an interesting subject to see the effects of lobes and sharp corners. Effect of radius on the intersections of lobes might be another topic to be investigated.

References

- [1] Bu, X., Peng, L., Lin, G., Bai, L., & Wen, D. (2015). Experimental study of jet impingement heat transfer on a variable-curvature concave surface in a wing leading edge. *International Journal of Heat and Mass Transfer*, *90*, 92-101.
- [2] O'Donovan, T. S., & Murray, D. B. (2007). Jet impingement heat transfer—Part I: Mean and root-mean-square heat transfer and velocity distributions. *International Journal of Heat and Mass Transfer*, *50*(17), 3291-3301.
- [3] O'Donovan, T. S., & Murray, D. B. (2007). Jet impingement heat transfer—Part II: A temporal investigation of heat transfer and local fluid velocities. *International Journal of Heat and Mass Transfer*, *50*(17), 3302-3314.
- [4] Carlomagno, G. M., & Ianiro, A. (2014). Thermo-fluid-dynamics of submerged jets impinging at short nozzle-to-plate distance: a review. *Experimental Thermal and Fluid Science*, *58*, 15-35.
- [5] Zhu, X. W., Zhu, L., & Zhao, J. Q. (2017). An in-depth analysis of conjugate heat transfer process of impingement jet. *International Journal of Heat and Mass Transfer*, *104*, 1259-1267.
- [6] Han, B., & Goldstein, R. J. (2001). (Han & Goldstein, 2001). *Annals of the New York Academy of Sciences*, *934*(1), 147-161.
- [7] Bouchez, J.-P., & Goldstein, R. (1975). Impingement cooling from a circular jet in a cross flow. *International Journal of Heat and Mass Transfer*, *18*(6), 719-730.
- [8] Jambunathan, K., Lai, E., Moss, M., & Button, B. (1992). A review of heat transfer data for single circular jet impingement. *International Journal of Heat and Fluid Flow*, *13*(2), 106-115.
- [9] Glynn, C., O'Donovan, T., & Murray, D. B. (2005). *Jet impingement cooling*. Paper presented at the Proceedings of the 9th UK National Heat Transfer Conference, Manchester, England, September.
- [10] San, J.-Y., Huang, C.-H., & Shu, M.-H. (1997). Impingement cooling of a confined circular air jet. *International Journal of Heat and Mass Transfer*, *40*(6), 1355-1364. doi:[http://dx.doi.org/10.1016/S0017-9310\(96\)00201-3](http://dx.doi.org/10.1016/S0017-9310(96)00201-3)
- [11] Yan, X., & Saniei, N. (1997). Heat transfer from an obliquely impinging circular air jet to a flat plate. *International Journal of Heat and Fluid Flow*, *18*(6), 591-599. doi:10.1016/S0142-727X(97)00051-9
- [12] Jennerjohn, M., Lee, J., Ren, Z., Ligrani, P., McQuilling, M., Fox, M. D., & Moon, H.-K. (2016). JET ARRAY IMPINGEMENT COOLING LOCAL NUSSELT NUMBER VARIATIONS: EFFECTS OF HOLE ARRAY SPACING, JET-TO-TARGET PLATE DISTANCE, AND REYNOLDS NUMBER. *47*(2), 119-140. doi:10.1615/HeatTransRes.2015011198
- [13] Colucci, D. W., & Viskanta, R. (1996). Effect of nozzle geometry on local convective heat transfer to a confined impinging air jet. *Experimental Thermal and Fluid Science*, *13*(1), 71-80. doi:10.1016/0894-1777(96)00015-5
- [14] Gulati, P., Katti, V., & Prabhu, S. V. (2009). Influence of the shape of the nozzle on local heat transfer distribution between smooth flat surface and impinging air jet. *International Journal of Thermal Sciences*, *48*(3), 602-617. doi:10.1016/j.ijthermalsci.2008.05.002
- [15] Herrero Martin, R., & Buchlin, J. M. (2011). Jet impingement heat transfer from lobed nozzles. *International Journal of Thermal Sciences*, *50*(7), 1199-1206. doi:10.1016/j.ijthermalsci.2011.02.017
- [16] Sodjavi, K., Montagné, B., Bragança, P., Meslem, A., Bode, F., & Kristiawan, M. (2015). Impinging cross-shaped submerged jet on a flat plate: a comparison of plane and hemispherical orifice nozzles. *Meccanica*, *50*(12), 2927-2947.
- [17] Kanamori, A., Hiwada, M., Oyakawa, K., & Senaha, I. (2011). Effect of orifice shape on flow behavior and impingement heat transfer. *Triangle*, *3*(39.7), 19.18.
- [18] Georgiadis, N. J., Debonis, J.R. (2006) Navier-Stokes analysis methods for turbulent jet flows with application to aircraft exhaust nozzles, *Progress in Aerospace Sciences.*, Vol. 42, p.377–418, 2006
- [19] ANSYS Inc (2009). *Fluent Theory Guide*, ANSYS Inc.
- [20] Behnia, M., Parneix, S., and Durbin, P. (1997). Accurate modeling of impinging jet heat transfer, Center for Turbulence Research Annual Briefs, p. 154,162, 1997
- [21] Schliinder, E.U., and Gnielinski, V., (1967). Warm e- und Stoffübertragung zwischen Gut und aufprallendem Diisenstrahl, *Chemie-Ing. Tech.*, *39*, 578-583 , 1967
- [22] Martin, H.,(1977). Heat and Mass Transfer Between Impinging Jets and Solid Surfaces, *Advances in Heat Transfer*, Vol. 13, 1977, pp. 1-60

- [23]Hollworth, B. R., (1985), Entrainment Effects on Impingement Heat Transfer: Part II—Local Heat Transfer Measurements, *Journal of Heat Transfer*, Vol. 107pp. 910-915, 1985.
- [24]Buchlin, J. M. (2011). Convective Heat Transfer in Impinging- Gas- Jet Arrangements, *Journal of Applied Fluid Mechanics*, Vol. 4, No. 2, Issue 1, pp. 137-149, 2011.